

# Energy Consumption and Thermal Comfort in Dwelling-cells: A Zonal-model Approach

C. INARD\*†  
 A. MESLEM\*  
 P. DEPECKER‡

(Received 26 May 1997; revised 8 September 1997; accepted 3 December 1997)

*In this study, we present a simplified model of the thermal behaviour of dwelling-cells, with a view to evaluating the performances of various heating systems that are commonly used in such environments. This model is based on a zonal-method representation of thermal exchanges in enclosed spaces.*

*Following the validation of the model, we carried out a numerical study on two types of heat source, i.e. localized (a hot-water radiator and an electrical convector) and distributed (a hot-water heated floor and an electrical heated ceiling).*

*The models were used to predict the heat losses specific to each system, as well as the indoor thermal ambience that the different systems induced. It was found that, for the configurations studied, the distributed heat sources presented a slight advantage over the localized sources, with regard to the criteria of energy consumption and thermal comfort. © 1998 Elsevier Science Ltd. All rights reserved.*

## NOMENCLATURE

$A$	surface convective exchange coefficient of radiator ( $\text{W m}^{-(1+\alpha)} \text{K}^{-d}$ )
$A_f$	façade area ( $\text{m}^2$ )
$C_p$	specific heat ( $\text{J kg}^{-1} \text{K}^{-1}$ )
$E_0$	plume entrainment constant
$F$	shape factor
$g$	gravitational acceleration ( $\text{m s}^{-2}$ )
$H_c$	height of the heat source (m)
$h_c$	surface convective exchange coefficient ( $\text{W m}^{-2} \text{K}^{-1}$ )
$J$	radiosity ( $\text{W m}^{-2}$ )
$K$	thermal conductance ( $\text{W m}^{-2} \text{K}^{-1}$ )
$L_c$	length of the heat source (m)
$m$	radiator water mass flow ( $\text{kg s}^{-1}$ )
$m(z)$	air mass flow ( $\text{kg m}^{-1} \text{s}^{-1}$ )
$nach$	air changes per hour ( $\text{h}^{-1}$ )
$Nu$	Nusselt's number
$P_{conv}$	convective power (W)
$Pr$	Prandtl's number
$P_{radf}$	radiative power (front of radiator) (W)
$P_{radb}$	radiative power (back of radiator) (W)
$Q(z)$	heat flux in the plume ( $\text{W m}^{-1}$ )
$Q_i$	flux transmitted through the façade (W)
$Q_v$	ventilation losses (W)
$R_a^*$	modified Rayleigh's number
$T$	temperature ( $^{\circ}\text{C}$ )
$T_a$	air temperature ( $^{\circ}\text{C}$ )
$T_f$	façade surface temperature ( $^{\circ}\text{C}$ )
$T_m$	maximum air temperature in the plume ( $^{\circ}\text{C}$ )
$T_{mr}$	mean radiant temperature ( $^{\circ}\text{C}$ )

$T_o$	operative temperature ( $^{\circ}\text{C}$ )
$T_{out}$	outdoor temperature ( $^{\circ}\text{C}$ )
$T_p$	mean air temperature in the plume ( $^{\circ}\text{C}$ )
$T_{su}$	water supply temperature ( $^{\circ}\text{C}$ )
$T_v$	ventilation temperature ( $^{\circ}\text{C}$ )
$T_w$	surface temperature ( $^{\circ}\text{C}$ )
$U$	surface transmission coefficient ( $\text{W m}^{-2} \text{K}^{-1}$ )
$V$	room volume ( $\text{m}^3$ )
$x, y, z$	coordinates (m)

## Greek symbols

$\beta$	volumetric expansion coefficient ( $\text{K}^{-1}$ )
$\Delta T_m$	maximum excess temperature in the plume ( $^{\circ}\text{C}$ )
$\Delta x, \Delta y$	discretization step along the $x$ or $y$ axis (m)
$\delta$	Kronecker's symbol
$\varepsilon$	emissivity
$\lambda$	thermal conductivity ( $\text{W m}^{-1} \text{K}^{-1}$ )
$\nu$	kinematic viscosity ( $\text{m}^2 \text{s}^{-1}$ )
$\rho$	density ( $\text{kg m}^{-3}$ )
$\sigma_0$	Stefan-Boltzmann's constant ( $\text{W m}^{-2} \text{K}^{-4}$ )
$\varphi_{cond}$	conductive heat flux density ( $\text{W m}^{-2}$ )
$\varphi_{conv}$	convective heat flux density ( $\text{W m}^{-2}$ )
$\varphi_{net}$	net radiative heat flux density ( $\text{W m}^{-2}$ )

## 1. INTRODUCTION

In order to predict the energy consumption levels and thermal comfort of heated spaces, it is necessary to take into account a number of parameters, e.g. the type of heating system used, the amount of insulation, the rate of air change and the external temperature.

As regards energy consumption, any evaluation of this factor must of course take account of thermal losses resulting from the type of heat source used. These losses are mainly conditioned by the radiative and convective

\* LEPTAB, Université de La Rochelle, Bât. des Sciences et Technologies, av. Marillac, F17042 La Rochelle Cedex 1, France.  
 † CETHIL, INSA, Bât. 307, 20 av. Einstein, F69621 Villeurbanne Cedex, France.  
 ‡ Tel.: 00335 4645 8203. Fax: 00335 4645 8241.

couplings between the heat source and the heat-losing surfaces, and by the thermal stratification of the air inside the dwelling-cell.

Concerning the type and the position of the heat source, it can be noticed that the ASHRAE procedure [1] ignores them whereas the CIBSE [2] includes the first item by considering the proportion of convective to radiant output of the emitter. In the French standard method [3], the type of heat source is taken into account with a heat source efficiency whose value is equal to 1.00 for a heating floor and to 0.95 for all other heating systems.

As to thermal comfort, an overall estimation at a number of points in the dwelling-cell can be carried out by the calculation of the PMV (Predicted Mean Vote) and PPD (Predicted Percentage of Dissatisfied) [4]. However, an overall analysis of this kind is generally not of itself sufficient, given the existence of local risks of discomfort due to the heterogeneity of surface temperatures (effects of cold surfaces and of radiation from the heat source), the thermal stratification of the indoor air, and cold air currents (natural convection along cold surfaces, and ventilation).

Numerous experimental studies [5–8] have made it possible to evaluate the performances of different heat sources with regard to energy consumption and thermal comfort, overall as well as local. But such studies, even though they are extremely useful, and also quite realistic, are unwieldy and costly. In the kind of context we are interested in, it is not possible to carry out systematic parametric studies, and in particular studies on the way in which heat is emitted. We therefore turned to the principle of simplified modelling, which, after the validation of a model, opened up the way to the numerous numerical tests required for a comparative study of the performances of different heating systems.

It was from this perspective that, in the framework of the French research group GREC (Groupe de Recherche sur les Emetteurs de Chaleur), we set about constructing a simplified model for describing the thermal fields of dwelling-cells equipped with different types of heat source, giving us the possibility of dealing with different ways in which heat is emitted. In specific terms, we developed zonal models based on a dividing-up of the interior volume of a dwelling-cell into zones.

To begin with, we developed models of heat sources, which we then coupled to models for calculating thermal exchanges within dwelling-cells.

## 2. MODEL OF HEAT SOURCES

The heat sources that we used fell into two categories, i.e. localized sources and distributed sources.

The localized heat sources were :

- a two-panel hot-water radiator, and
- an electrical convector with frontal delivery.

The distributed heat sources were :

- an electrical heated-ceiling system, and
- a hot-water heated-floor system.

### 2.1. Model of the hot-water radiator

This model is based on a primary hypothesis which stipulates that the flow of water through the radiator is modelled by a plug-flow method, i.e. the radiator is represented by the use of elements coupled in series. This implies that all the elements of the radiator receive the total flow passing through the radiator, and that the supply temperature of a given element is the same as the exhaust temperature of the previous element. This mode of representation has already been used successfully by a number of authors [9, 10], notably in the framework of Annex 10 of the International Energy Agency. Moreover, if the mean temperature of the liquid, in steady state, is close to the surface temperature of the radiator, we can neglect the effects of convection between the water and the metal, as well as those of conduction through the metal itself. We also make the working hypothesis that the exhaust temperature of the water from an element is the representative temperature of this element. This hypothesis requires that, for the accurate representation of the drop in temperature of the water within the radiator, there be a sufficient discretization of the radiator (into at least four elements [10]). Taking all of these factors together, the thermal balance, in steady state, of a given element  $i$  of the radiator is expressed thus :

$$P_{\text{radf}_i} + P_{\text{radb}_i} + P_{\text{conv}_i} = mC_p(T_{i-1} - T_i) \quad (1)$$

The convective power of the element  $i$  is :

$$P_{\text{conv}_i} = AL_e H_c (T_i - T_a)^d \quad (2)$$

where  $P_{\text{conv}_i}$  is the total convective power from all the four radiator surfaces.

The coefficients  $A$ ,  $c$  and  $d$  were experimentally measured, in steady state, for several types of hot-water radiator [11]. The values obtained for the radiator of the double-panel type that we used in this study were, respectively, 8.63, 0.75 and 1.22.

The back radiative power calculations were carried out on the assumption that the shape factor between the back of the heat source and the wall behind it was equal to one and the front radiative power is computed using the method of radiosities (see Section 3.2).

### 2.2. Model of the electrical convector

The proposed model of the convector is very simple, being based on the observation that convector technology differs little between one manufacturer and another.

The equations featuring in this model, which were derived from a statistical study [12], were used to calculate the variables of the coupling between the heat sources and the heated space, i.e. the temperatures at the front ( $T_{\text{wcf}}$ ) and the back ( $T_{\text{wcb}}$ ) of the convectors. The study made use of data bases compiled from 200 tests carried out at nominal power at the Laboratoire Central des Industries Electriques (LCIE), as well as 16 tests carried out at partial load at the Centre Technique des Industries Aérauliques et Thermiques (CETIAT), the Centre Scientifique et Technique du Bâtiment (CSTB) and the Laboratoire National d'Essais (LNE).

Thus, for frontal-delivery electrical convectors, the front and back surface temperatures were expressed as (see Fig. 1) :

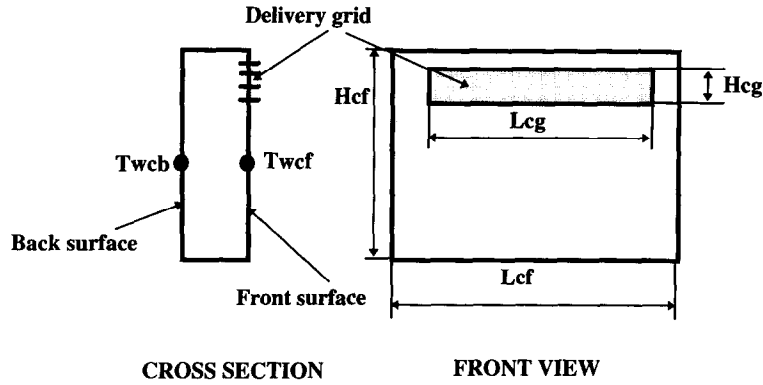


Fig. 1. View of the electrical convector.

$$T_{wcf} = \frac{P_{elec}}{P_{nom}A_{cf}} [0.77\Delta T_{a\max}A_{cg} + 0.67\Delta T_{wcf\max}(A_{cf} - A_{cg})] + T_a \quad (3)$$

$$T_{wcb} = \frac{P_{elec}}{P_{nom}} (0.67\Delta T_{wcf\max} - 7) + T_a \quad (4)$$

with :

$A_{cf}$	front surface of the convector ( $L_{cf} \times H_{cf}$ )
$A_{cg}$	surface of the delivery grid ( $L_{cg} \times H_{cg}$ )
$L_{cf}$	front surface length
$H_{cf}$	front surface height
$L_{cg}$	delivery grid length
$H_{cg}$	delivery grid height
$\Delta T_{a\max}$	maximum excess in convector air delivery temperature (normalized test)
$\Delta T_{wcf\max}$	maximum heating at the front of the convector (normalized test)
$P_{nom}$	nominal electrical power of the convector (maximum electrical power)
$P_{elec}$	electrical power consumed by the convector (actually consumed power : partial load).

We used the results of the normalized tests ( $P_{nom}$ ,  $\Delta T_{a\max}$  and  $\Delta T_{wcf\max}$ ) and of the electrical power supplied ( $P_{elec}$ ) to determine the values of the convector's front and back surface temperatures. These values were then used to calculate the convector's radiative power using the method of radiosities (see Section 3.2) which, when subtracted from the electrical power, gave its convective power.

### 2.3. Electrical heated-ceiling model

The electrical heated-ceiling model was based on the utilization of the method of finite differences. A study carried out by the CSTB [13] has shown that, from the point of view of heat emission as well as that of thermal comfort, a one-dimensional model satisfies the objectives set out, i.e. to analyze energy consumption and thermal comfort. It should be pointed out that only results in steady state conditions are presented in this paper ; nevertheless, transient simulations using the finite difference

method have been performed. The thermal balance of the node  $i$ , in steady state, is expressed as (see Fig. 2) :

$$K_{ij}(T_i - T_j) + K_{ik}(T_i - T_k) = 0 \quad (5)$$

In the general case, the thermal conductance,  $K_{ij}$ , between the nodes  $i$  and  $j$ , is :

$$K_{ij} = \frac{2\lambda}{\Delta x_i + \Delta x_j} \quad (\text{W m}^{-2} \text{K}^{-1})$$

The radiative and convective power were decoupled ; the convective emission law used for this purpose is given in Section 3.1.

### 2.4. Hot-water heated-floor model

The hot-water heated-floor model that we opted for was also based on the use of the finite difference method. For this type of distributed heating system, a two-dimensional discretization is needed in order to evaluate correctly its thermal behavior. The establishment of the thermal balance at each discretization node, in steady state, produces a system of equations whose unknown variables are the temperatures. For example, as regards the node  $i$  we write (see Fig. 3) :

$$K_{ij}(T_i - T_j) + K_{ik}(T_i - T_k) + K_{il}(T_i - T_l) + K_{im}(T_i - T_m) = 0 \quad (6)$$

In the general case, the thermal conductances between the nodes are expressed as :

—along the  $x$  axis :

$$K_{ij} = \frac{2\Delta y_i \lambda}{\Delta x_i + \Delta x_j} \quad (\text{W m}^{-1} \text{K}^{-1})$$

—along the  $y$  axis :

$$K_{im} = \frac{2\Delta x_i \lambda}{\Delta y_i + \Delta y_m} \quad (\text{W m}^{-1} \text{K}^{-1})$$

As to the temperature of the heating water, it was calculated on the basis of the thermal balance of the water volume, and on the assumption that it was equal to the arithmetic mean of the supply and exhaust temperatures. We then calculated the mean interior and exterior surface temperatures of the floor, using the flux conservation equations for these surfaces. In this case,

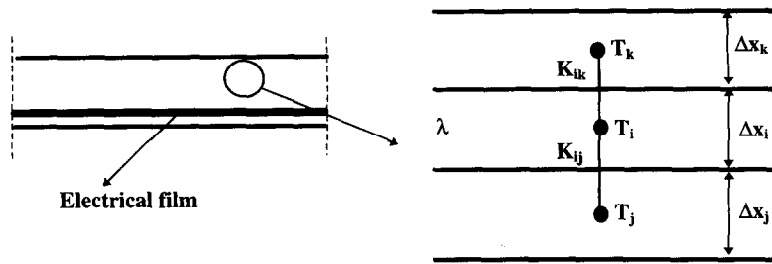


Fig. 2. Sketch of the heating ceiling.

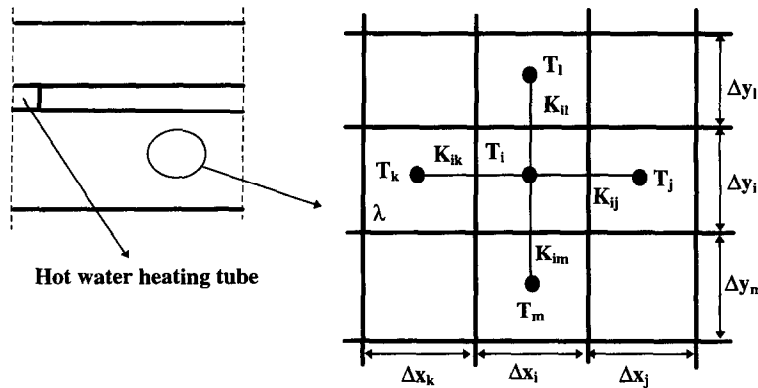


Fig. 3 Sketch of the heating floor.

too, the radiative and convective powers were decoupled ; the convective emission law used for this purpose is given in Section 3.1.

All these models were integrated into the overall model used for evaluating the thermal exchanges within the heated space, as described below.

### 3. MODELLING OF THERMAL EXCHANGES WITHIN THE DWELLING-CELL

Here we are concerned with a problem of coupled heat transfers, where the three different modes of heat transfer appear simultaneously : convective transfers in the indoor air volume, radiative transfers between the different surfaces of the enclosed space, and conductive transfers through the walls.

#### 3.1. Modelling of convective exchanges

The model has to be able to represent a heated space with respect to the different types of heat source used, which are characterized by extremely diverse modes of heat emission. For those of the first category (localized heat sources), the driving flow is the thermal plume produced by the heat source, while for those of the second (distributed heat sources) this role is played by the cold boundary layers that develop along the walls.

The modelling of the convective exchanges must take account of this difference. In order to do so, we propose to distinguish between the two types of heat source by using two different schemas of indoor air flow, as shown in Figs 4 and 5.

First, we set out, for each zone, the mass and thermal balances. To express the closing of the problem, it is

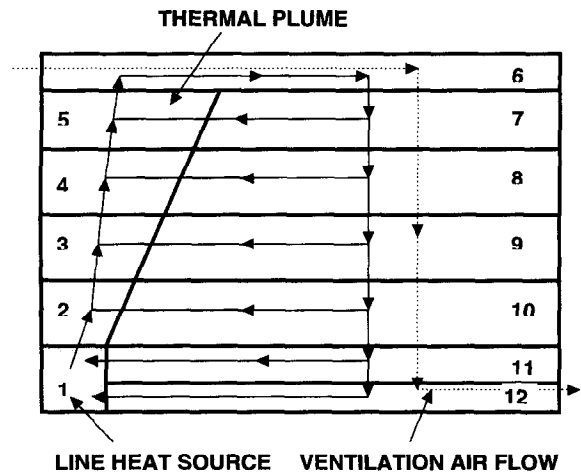


Fig. 4. Thermoconvective schema used for the localized heat sources.

necessary to know the mass air flows between the zones, and also the convective heat fluxes at the walls.

The mass air flow of the thermal plume of the localized heat sources was calculated on the assumption that the sources behaved in a linear way.

Thus, mass air flow is expressed as follows [14]:

$$m(z) = 0.1E_0Q(z)^{1/3}z \quad (7)$$

For hot-water radiators, the linear behavior of the thermal plume has already been established [15, 16]. For all that, the authors showed that the velocity and temperature profiles in the thermal plumes issued from hot-

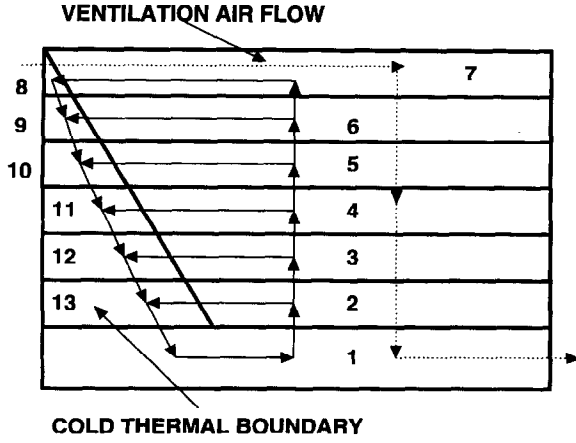


Fig. 5. Thermoconvective schema used for the distributed heat sources.

water radiators are similar to those from a linear heat source.

We used a study carried out on the thermal plume associated with hot-water radiators to identify the value of the plume entrainment constant  $E_0$  [16]. It came out at 0.09. As to front-delivery convectors, the value of  $E_0$  calculated on the basis of an experimental study carried out at CETIAT [17] was 0.14.

Finally, for the mass air flow of the cold thermal boundary layers, we used the experimental results obtained by Allard *et al.* [18], which can be expressed in the following form :

$$m(z) = 0.004(T_a - T_w)^{1/3} z \quad (8)$$

The calculation of convective heat fluxes at the walls must take account of the specificities of the different heating systems, and, notably, the particular convective couplings between heat sources and walls. This is why we distinguish not only between the different types of heat source, but also between the different walls. Thus, the convective heat flux exchanged at the wall behind a localized heat-source is expressed as follows [11] (see Fig. 6) :

$$\varphi_{\text{conv}} = \frac{1.83}{H_c^{0.25}} \left( \frac{T_{\text{wb}} + T_{\text{we}}}{2} - T_a \right)^{1.25} \quad (9)$$

This correlation brings in the mean surface tem-

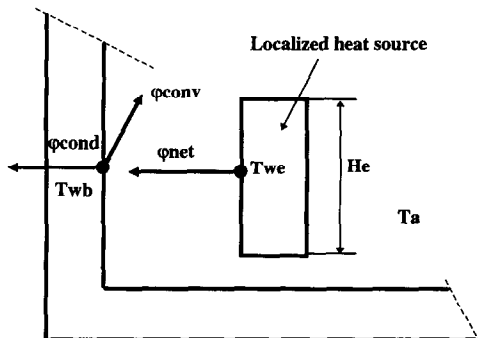


Fig. 6. Heat fluxes exchanged between a localized heat source and the wall behind.

perature of the wall behind the heat source ( $T_{\text{wb}}$ ), and also that of the back of the source ( $T_{\text{we}}$ ). It is to be noted that this correlation is very close to that obtained by Olusoji and Hetherington [19] for the calculation of the convective heat flux exchanged along an open vertical channel. The radiative heat flux density  $\varphi_{\text{net}}$  is computed identically to the radiator as explained in Section 2.1.

The convective flux exchanged along the plumes of electrical convectors is calculated by the use of an experimental correlation derived from experiments carried out at CETIAT [17], expressed as follows :

$$\varphi_{\text{conv}}(z) = 0.66(\Delta T_m + T_a - T_w)^{1.77} \quad (10)$$

The maximum temperature excess in the plume ( $\Delta T_m$ ) is calculated on the basis of the asymptotic solution for a thermal plume from a linear source, developing along an isothermal wall [14] :

$$\Delta T_m(z) = 5.37 \left( \frac{Q(z)g\beta}{\rho C_p} \right)^{2/3} \frac{1}{g\beta z} \quad (11)$$

$\Delta T_m(z)$  is used to compute the convective heat flux density exchanged between the thermal plume and the wall [eqns (10), (17) and (18)].

The expression used for the plumes associated with hot-water radiators is somewhat different. Having shown that the dynamic and thermal structure of this type of flow is analog to that of the thermal plume from a linear heat source, we made use of a correlation obtained by Liburdy and Faeth [14], who put forward the following law :

$$Nu(z) = 1.344 Ra(z)^{*0.18} \quad (12)$$

with  $Nu(z)$  being the local Nusselt's number, and  $Ra(z)^*$  being the local modified Rayleigh's number.

The local Nusselt's number is defined thus :

$$Nu(z) = \frac{h_c(z)z}{\lambda} \quad (13)$$

The local modified Rayleigh's number is expressed thus :

$$Ra(z)^* = \frac{g\beta Q(z)z^3}{\lambda v^2} Pr \quad (14)$$

As to the heat flux in the plume,  $Q(z)$ , its expression [14] is :

$$Q(z) = Q(H_e) \left( \frac{H_e}{z} \right)^{0.14} \quad (15)$$

where  $Q(H_e)$  is the heat flux in the plume at  $z = H_e$  i.e. the sum of the convective power of the heat source and the convective heat flux from the wall behind the heat source.

Replacing  $Nu(z)$  and  $Ra(z)^*$  in (12), and  $Q(z)$  in (14), by their expressions gives :

$$h_c(z) = 1.8Q(H_e)^{0.18} H_e^{0.0245} z^{-0.484} \quad (16)$$

$h_c(z)$  is the convective exchange coefficient between the thermal plume and the wall.

Using the zonal model, we calculated a mean air temperature for the plume, and it was interesting to compare

Table 1. Values of the coefficients  $a$  and  $b$  used for the evaluation of the coefficients of the convective exchange

Wall	Localized heat source	Distributed heat source
Ceiling	$a = 3$ $b = 0.66$ [11]	$a = 0.2$ $b = 1/4$ [22]
Floor	$a = 1$ $b = 0$ [20]	$a = 1.5$ $b = 1/3$ [23]
Vertical wall	$a = 3$ $b = 1/3$ [21]	$a = 1.45$ $b = 1/3$ [24]

the convective heat flux density to the mean temperature difference. It has already been shown [16] that with the thermal plumes of hot-water radiators the velocity and temperature profiles are similar. Our analysis of temperature profiles shows that :

$$\frac{T_p(z) - T_a(z)}{T_m(z) - T_a(z)} \approx 0.71 \quad (17)$$

with  $T_p(z)$  being the mean air temperature in the plume at height  $z$ , and  $T_m(z)$  being the maximum air temperature in the plume at height  $z$ .

The local density of the convective heat flux is then expressed as :

$$\varphi_{\text{conv}}(z) = \frac{h_c(z)}{0.71} [T_p(z) - T_a(z)] + h_c(z)[T_a(z) - T_w(z)] \quad (18)$$

Finally, the convective heat fluxes at the other walls were evaluated using a correlation of the following type :

$$\varphi_{\text{conv}} = h_c(T_a - T_w) \quad (19)$$

with  $h_c = a(T_a - T_w)^b$

Table 1 brings together the values of  $a$  and  $b$  used, according to the type of wall and heat source.

It is interesting to note that this model of the convective exchanges allows us to compute, in particular, the indoor air temperature stratification and the mean air speed in the enclosure.

### 3.2. Modelling of radiative exchanges

The net radiative heat fluxes were evaluated by the method of radiosities [25]. In order to take account of the inside surface temperature heterogeneity, the interior surface of the dwelling-cell was discretized into 95 elements (Fig. 7), which were taken as being isothermal. The establishment of the radiative balance for each surface was used to calculate the density of the corresponding net radiative heat flux :

$$\varphi_{\text{net},i} = \frac{\varepsilon_i}{1 - \varepsilon_i} (\sigma_0 T_{w_i}^4 - J_i) \quad (20)$$

The radiosity,  $J_i$ , of each surface, was evaluated by resolving the following linear system :

$$\sum_j [\delta_{ij} - (1 - \varepsilon_i)F_{ij}]J_j = \varepsilon_i \sigma_0 T_{w_i}^4 \quad (21)$$

Since we were working here with parallel and perpendicular surfaces, the shape factors  $F_{ij}$  could be estimated exactly [25].

Lastly, the heat balance of each interior surface  $i$  is expressed by :

$$\varphi_{\text{net},i} + \varphi_{\text{conv},i} + \varphi_{\text{cond},i} = 0 \quad (22)$$

Equation (22) is non-linear and an iterative procedure is used to solve it.

## 4. COMPARISON OF THE MODEL WITH EXPERIMENTAL RESULTS

We compared the results given by the model with those of experiments carried out in two test cells. More precisely, the comparison was between the measured and the calculated air temperature profiles inside the dwelling-cell.

The first experimental set-up to be tried out was CET-IAT's RAD1 cell, which was used for the determination of the nominal power of hot-water radiators. This cell, which measures  $4.0 \times 4.0 \times 2.8$  m, is cooled, on its six faces, by six independent climatic units. A detailed description of the RAD1 cell is given in [16].

In this cell, we tested a hot-water radiator of the double-panel type, with two levels of water-supply temperature ( $T_{\text{su}}$ ), i.e. 90 and 65°C, respectively. The tests were carried out without ventilation.

For the other three types of heat source (electrical convector, hot-water heated-floor system, and electrical heated-ceiling system), the tests were carried out in the CSTB's EREDIS cell. All the vertical walls of the cell except for the façade were well insulated, as was the ceiling, in order to limit conductive heat fluxes. The floor was equipped with water-circulation panels to simulate a heated-floor system. The façade itself was composed of circulating-water panels, which made it possible to set a surface temperature representative of the outside climate. The façade also included a breast-wall 1 m high, below the window, composed of a 2 cm layer of insulating material.

A detailed description of the EREDIS cell is given in [26].

The cell possesses an air-change system whose inlet is at the top of the façade, in the median plane of the cell. The exhaust is situated at floor level in the wall opposite to the façade.

Concerning the tests that are relevant to present purposes, the rate of air change was set at 0.5 ach, with air temperatures ( $T_v$ ) of +8 and +12°C, respectively. The surface temperatures of the façade ( $T_f$ ) were set at +12 and +15°C, respectively.

Figures 8–11 give the results obtained for all the different heat sources, from which it can be seen that the model correctly reproduces the measured vertical air temperature profiles. Thus, for the occupancy zone, the maximum difference between measurements and calculations comes out at 0.8°C. This allows us to take the study a step further.

In sum, these simulations were carried out in order to evaluate the performances of heat sources with regard to energy consumption and thermal comfort.

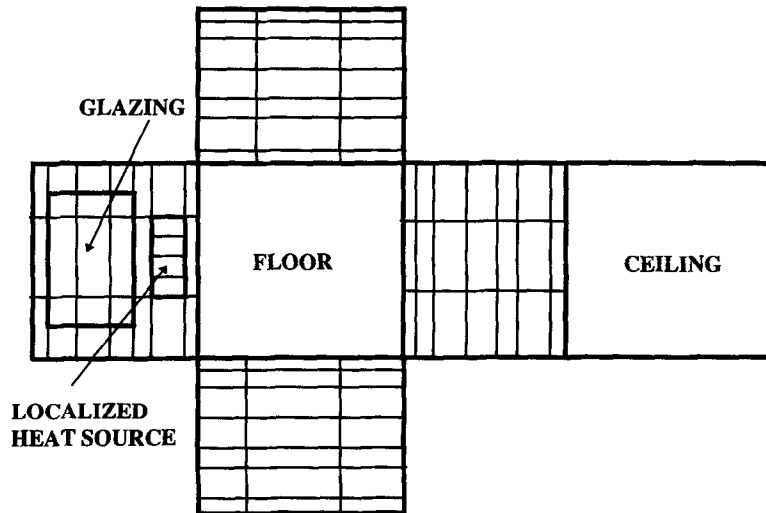


Fig. 7. Discretization of the interior surface of the dwelling-cell.

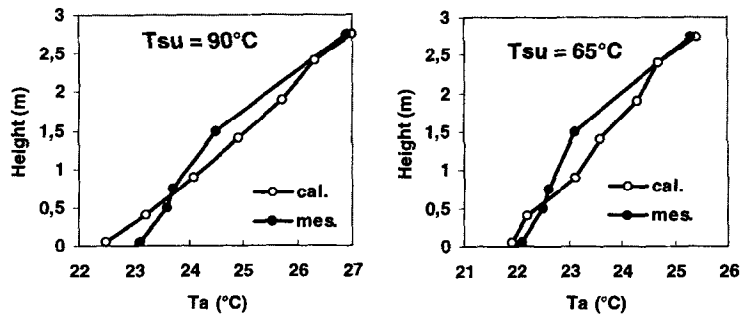


Fig. 8. Vertical profiles of air temperature, measured and calculated (hot-water radiator).

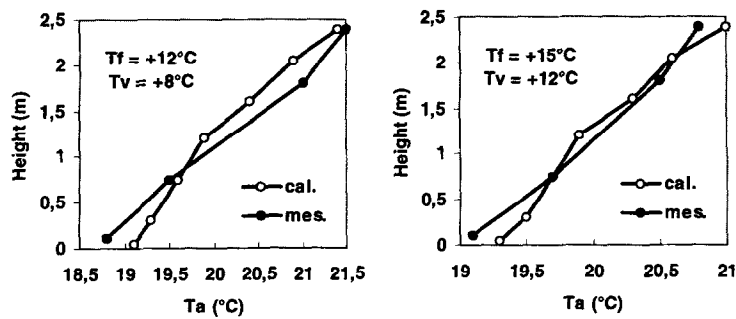


Fig. 9. Vertical profiles of air temperature, measured and calculated (electrical convector).

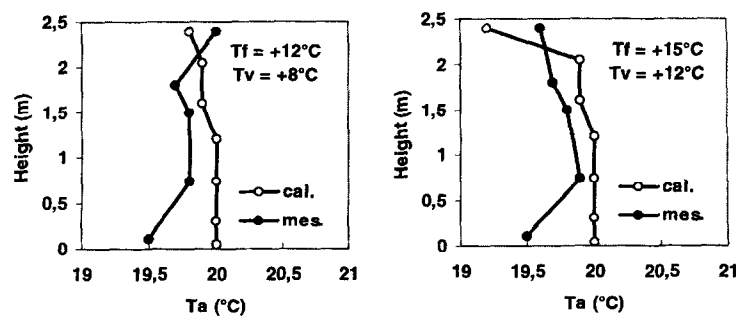


Fig. 10. Vertical profiles of air temperature, measured and calculated (hot-water heated floor).

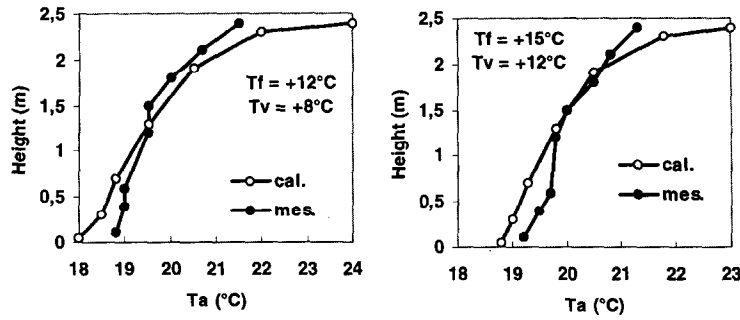


Fig. 11. Vertical profiles of air temperature, measured and calculated (electrical heated ceiling).

5. CASES TREATED

We chose a configuration corresponding to a living-room of 4.0 × 5.0 × 2.5 m in an apartment situated at mid-height in a block, with just the façade in contact with the exterior, the other walls being in contact with premises heated to the same temperature as the environment under consideration. Figure 12 gives a view of the dwelling-cell studied. The heat sources were :

- an electrical convector with frontal delivery ;
- a two-panel high-temperature water radiator ;
- a two-panel low-temperature water radiator ;
- a hot-water heated-floor system ;
- an electrical heated-ceiling system.

The localized heat sources were placed either beneath the window or on the opposite wall. Figure 13 shows the different heating configurations studied.

The façade, measuring 5.0 × 2.5 m, had a glazed part measuring 2.10 × 1.25 m, below which was a breast-wall 1.0 m high. We looked at three levels of insulation of the façade, i.e. badly insulated, minimally insulated and well insulated. Figure 14 shows a cross section of the façade.

Table 2 gives the values of the coefficients of surface transmission of the façade, calculated according to the ASHRAE method [1].

Ventilation was taken care of by an inlet situated above the glazed part, the exhaust being at floor level on the wall opposite the façade. The rate of air change nach was set at 0.8 ach, and the inlet temperature was the same as the outside temperature.

The simulations were carried out at four levels of power, corresponding to four values of the outside temperature:  $T_{out} = -15, -5, +5, +15^{\circ}C$ . Thus, and considering the three levels of insulation, the total number of simulations carried out was 96.

In order to make valid comparisons between the different results, the supplied power (in terms of electrical wattage or supply water temperature) was adjusted in such a way that for all the different simulations there was an operative temperature, at the center of the dwelling-unit, of  $20 \pm 0.04^{\circ}C$ , using the formula :

$$T_o = \frac{T_{mr} + T_a}{2} \tag{23}$$

$T_{mr}$  is the mean radiant temperature which is computed as follows :

$$T_{mr} = \left( \frac{\sum_j F_{cj} J_j}{\sigma_o} \right)^{1/4} - 273.15 \tag{24}$$

where  $F_{cj}$  is the shape factor between the sensor and the surface  $i$  [25].

Equation (23) is a simplified expression of  $T_o$ ; it is authorized by the international standard ISO 7730 [4] for the thermal configurations that concern us here.

The aim of these numerical tests was to compare the performances of different heating systems. In order to achieve this, we had to decide on criteria of comparison. These were, of course, expressed in terms of energy consumption, but also in terms of thermal comfort, which we

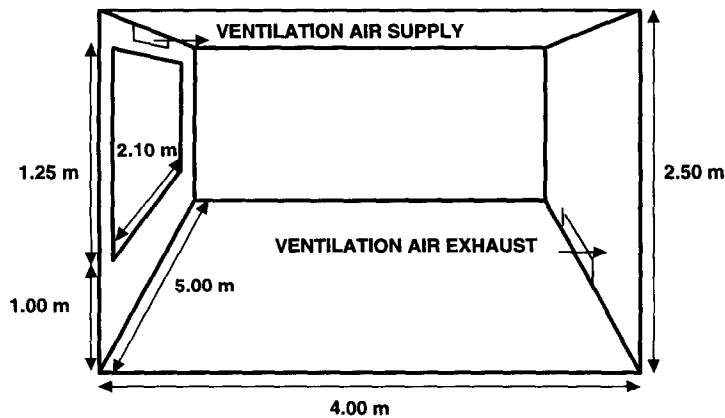


Fig. 12. View of the dwelling unit studied.

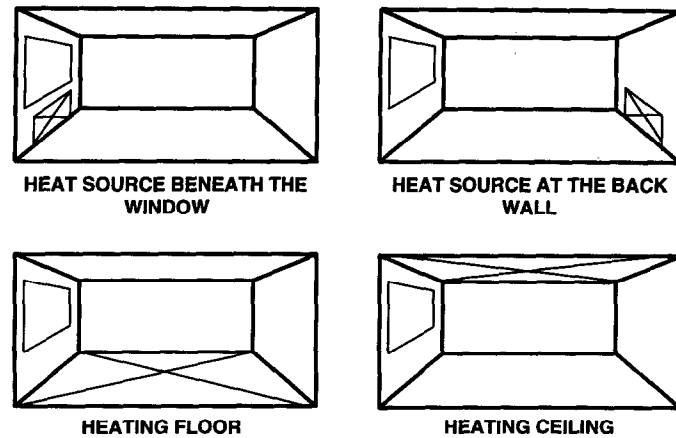


Fig. 13. Heating configurations studied.

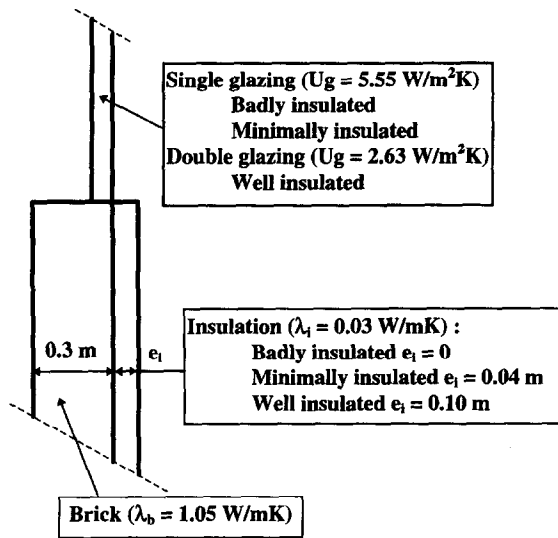


Fig. 14. Cross section of the façade.

Table 2. Values of the façade transmission coefficient

Level of insulation	$U$ (W/m <sup>2</sup> K)
Bad	2.98
Minimum	1.62
Good	0.76

decided to evaluate in line with the international standard ISO 7730 [4]. This standard takes into account overall thermal comfort, through the PMV and PPD indices, as well as the idea of local discomfort, measured by:

- the vertical difference in air temperature between 0.1 and 1.1 m above the floor, which must be less than 3 K ;
- the floor temperature, which must be between 19 and 26°C, the maximum permitted temperature being 29°C for a heated-floor system ;

- the horizontal asymmetry of radiation at a height of 0.6 m, which must be less than 10 K ;
- the vertical asymmetry of radiation at a height of 0.6 m, which must be less than 5 K ;
- the mean air speed, which must be less than 0.15 m/s.

We evaluated all these criteria for different points in the occupancy zone, i.e. at distances not less than 0.3 m from the vertical walls and heights not more than 1.7 m above the floor. Furthermore, the calculations were carried out on 15 verticals, for heights of 0.1, 0.6, 1.1 and 1.7 m.

The determination of the PMV index was carried out for a person wearing indoor clothing suitable for winter conditions (1.0 clo), and with a low level of activity (1.2 met).

The calculation of this index also included the assumption that the partial pressure of water vapor was known, although in fact this value was not calculated by the model. However, it is a parameter which in winter conditions, in temperate climates, has only a slight influence on PMV values [4]. We therefore set the hygrometric level to 50%, which, given the indoor air temperature values we were working with, was within the range of the partial water vapor pressure advocated by the ISO 7730 standard.

Finally, the mean air speed was evaluated by dividing the flow of air between two adjacent zones by the area of the interface between the zones in question.

Using the PMV values, the PPD index is expressed as follows [4] :

$$PPD = 100 - 95 e^{-(0.03533PMV^4 + 0.2179PMV^2)} \quad (25)$$

## 6. ANALYSIS OF THE RESULTS: COMPARISON OF THE DIFFERENT HEATING SYSTEMS

Before moving on to a comparative study as such, we analyzed the impact of each type of heat source on the indoor ambience. We did this using, on the one hand, the difference between the mean radiant temperature ( $T_{mr}$ ) and the air temperature ( $T_a$ ) at the center of the dwelling-cell, which quantified the radiative/convective aspect of heat emission, and, on the other hand, the vertical air

Table 3. Calculated values of  $(T_{mr} - T_a)$  for the different heating systems

Heating system	$T_{mr} - T_a$ (°C)		
	Mean	Minimum	Maximum
Heating floor	+0.6	+0.3	+1.3
Heating ceiling	+1.9	+0.5	+4.3
High-temperature water radiator	+0.3	0.0	+0.8
Low-temperature water radiator	+0.1	-0.5	+0.6
Electrical convector	-0.5	-1.4	0.0

temperature difference, which compounded the previous criterion with the idea of a particular mode of heat emission (localized vs distributed).

Table 3 gives the mean  $(T_{mr} - T_a)$  values for each heat source, and also the maximum and minimum values. The mean values are the average of all the simulations carried out for each heating system. Concerning the distributed heat sources, the minimum values were found for a good insulation and  $T_{out} = +15^\circ\text{C}$  whereas the maximum values were obtained for a bad insulation and  $T_{out} = -15^\circ\text{C}$ . For the localized heat sources, it was the opposite.

The results showed that for hot-water radiators the enclosure received a small amount of heat by direct radiation from the heat source, with a little more homogeneity for the low-temperature radiator. This radiative heating effect was much more significant with the distributed heat sources; the effect was especially marked with the heated ceiling, due to the fact that only a small amount of convective exchange took place at the heat source. Finally, for the electrical convector, we noted a slight radiative deficit, essentially due to cold radiation from the façade.

All these values are to be seen in the light of those which were found experimentally by Marret [27]:

—hot-water radiator:  $0 \leq (T_{mr} - T_a) \leq 0.4$  K

—distributed heat sources:  $0.7 \leq (T_{mr} - T_a) \leq 1.7$  K

—convective heating:  $-0.7 \leq (T_{mr} - T_a) \leq -0.2$  K

The other criterion used to study the influence of the type of heat source on the indoor ambience was the vertical air temperature difference at the center of the dwelling-cell.

Table 4 gives the mean, maximum and minimum values of  $(T_{a_{1,70m}} - T_{a_{0,10m}})$  for each heat source.

It is interesting to note that the two distributed heat sources are at the extremities of the recorded range of the mean differences, with the heated floor giving the lowest value. This can be explained by the fact that for this particular heat source, convective phenomena were of positive buoyancy, while for the heated ceiling they tended to be blocked. As to the localized heat sources, the electrical convector gave a higher mean value than the hot-water radiators. This was the result of its convective share of the overall power being larger. Finally, for the hot-water radiators, the slight observed difference

Table 4. Calculated values of  $(T_{a_{1,70m}} - T_{a_{0,10m}})$  for the different heating systems

Heating system	$T_{a_{1,70m}} - T_{a_{0,10m}}$ (°C)		
	Mean	Minimum	Maximum
Heating floor	0.0	-0.1	+0.1
Heating ceiling	+1.1	+0.2	+2.1
High-temperature water radiator	+0.6	0.0	+1.8
Low-temperature water radiator	+0.4	0.0	+1.4
Electrical convector	+1.1	+0.2	+2.7

between the high-temperature and low-temperature radiators was not due to the convective component of the power, which was virtually the same for the two heat sources (around 70%), but to the difference in the area of the heating surface.

All these figures, taken together, demonstrate the consistency that can be achieved by numerical methods with regard to physical phenomena brought about within a heated space.

We can now take up the question of establishing comparisons, properly speaking, between the different heat sources. As previously mentioned, these comparisons concern both energy consumption and thermal comfort.

#### 6.1. Analysis of energy consumption

As regards energy consumption, and in view of the configuration simulated, there are two components that need to be analyzed:

- heat fluxes through the façade;
- heat losses due to ventilation.

It is to be noted that, although the rate of air inlet flow was fixed, heat losses through ventilation varied according to the case studied, due to different air-temperature distributions.

Table 5 shows the mean values for the different outdoor temperature of heat fluxes through the façade ( $Q_t$ ), heat losses caused by ventilation ( $Q_v$ ), per heat source, and the following ratio:

$$R = \frac{\sum_{i=1}^3 (Q_t + Q_v)}{\left[ \sum_{i=1}^3 (Q_t + Q_v) \right]_{\min}} \quad (26)$$

In eqn (26), the index  $i$  corresponds to the three levels of insulation of the façade that were studied.

Furthermore, Table 6 gives the  $Q_{to}$  and  $Q_{vo}$  computed as follows [1]:

$$Q_{to} = UA_f(T_o - \bar{T}_{out}) \quad (27)$$

$$Q_{vo} = 1.2 \text{ nach } V \frac{1000}{3600} (T_o - \bar{T}_{out}) \quad (28)$$

with  $\bar{T}_{out}$  being the mean outdoor temperature equal to  $0^\circ\text{C}$ , and

To being the indoor operative temperature equal to  $20^\circ\text{C}$ .

Table 5. Mean values for heat losses at the façade and by ventilation for the different heating systems

Heating system	Badly insulated		Minimally insulated		Well insulated		<i>R</i>
	$Q_t$ (W)	$Q_v$ (W)	$Q_t$ (W)	$Q_v$ (W)	$Q_t$ (W)	$Q_v$ (W)	
	$\bar{T}_{out} = 0^\circ\text{C}$ $T_o = 20^\circ\text{C}$						
Heating floor	685	261	380	263	181	261	1.00
Heating ceiling	704	241	398	247	185	249	1.00
Electrical convector (window)	804	258	432	262	201	266	1.10
Electrical convector (backwall)	752	258	410	262	193	266	1.06
High-temperature water radiator (window)	790	261	424	264	198	267	1.09
High-temperature water radiator (backwall)	752	260	409	264	193	267	1.06
Low-temperature water radiator (window)	769	263	414	266	194	267	1.07
Low-temperature water radiator (backwall)	751	262	408	265	192	267	1.06

Table 6. Values of  $Q_{to}$  and  $Q_{vo}$ 

$\bar{T}_{out} = 0^\circ\text{C}$ $T_o = 20^\circ\text{C}$	Badly insulated	Minimally insulated	Well insulated
	$Q_{to}$ (W)	745	405
$Q_{vo}$ (W)	267	267	267

Table 5 calls for a number of comments. Firstly, it turns out that the minimum values of heat flux transmitted at the façade were obtained in every case with the heated floor, while those of heat losses by air ventilation were obtained with the heated ceiling. For heat losses through the façade, the distributed heat sources gave lower heat fluxes than the localized heat sources, with a slightly lower value for the heated floor due to a higher level of radiative coupling between the heated ceiling and the glazing.

As to the localized heat sources placed beneath the window, the values were higher on account of the strong thermal coupling between the façade and the heat source. When these same sources were positioned on the back wall, it was found that, as one might expect, slightly lower flux values were observed.

This finding is corroborated by the fact that the maximum values were obtained with the electrical convector (given the convective share of its output), while the lowest values were given by the low-temperature radiator (due to the lower temperature in its plume).

Comparing the  $Q_{to}$  and  $Q_t$  values, the same comments apply seeing that  $Q_{to}$  is computed with a constant surface transmission coefficient  $U$ .

As to heat losses through ventilation, it is firstly to be observed that, with the exception of the heated floor, which gave an almost-unvarying thermal gradient, there was always a slight increase in these heat losses with the level of insulation, due to a decrease in the thermal gradient of the indoor air. We would recall, at this point, that the supply of fresh air took place in the upper part of the dwelling-cell, while the exhaust took place at floor level. It is also interesting to note that, with the exception of the heated ceiling, these heat losses were all of a very similar order. This may at first sight appear surprising,

in view of the air temperature differences given in Table 4. However, if we take, for example, the cases of the heated ceiling and the electrical convector, which gave the same mean vertical air temperature difference, the disparity observed in terms of heat losses through ventilation was essentially due, not to the thermal gradient, but to the air temperature level inside the dwelling-cell (see Table 3).

All these findings also explain the differences between  $Q_{vo}$  and  $Q_v$  values.

As regards the values of the ratio  $R$ , it turns out that the two distributed heat sources (hot-water heated floor and electrical heated ceiling) gave the lowest values for heat losses. As to the localized heat sources, we observed a slight decrease in  $R$  when they were positioned on the back wall, though with the low-temperature water radiator the difference was very small, due to the degree of uniformity of its mode of heat emission (a large heated area and a low temperature of the heat source).

## 6.2. Analysis of thermal comfort

As regards thermal comfort, the indices chosen were the PPD and the criteria of local discomfort.

We looked first at overall thermal comfort.

Table 7 gives the mean and maximum PPD values for

Table 7. Values of the PPD index for the occupancy zone

Heating system	PPD mean (%)	PPD maximum (%)	n (PPD > 10%)
	Heating floor	7	16
Heating ceiling	9	27	176
Electrical convector (window)	7	12	14
Electrical convector (backwall)	7	14	27
High-temperature water radiator (window)	7	11	5
High-temperature water radiator (window)	7	12	31
Low-temperature water radiator (window)	7	13	25
Low-temperature water radiator (backwall)	8	14	39

Table 8. Number of points in the occupancy zone for which the local criteria of comfort were not satisfied

Heating system	$n(R_h)$	$n(R_v)$	$n(E)$	$n(S)$	$n(C)$
Heating floor	1	8	0	0	45
Heating ceiling	1	0	0	0	60
Electrical convector (window)	9	3	0	0	0
Electrical convector (backwall)	10	1	0	0	0
High-temperature water radiator (window)	6	1	0	0	0
High-temperature water radiator (backwall)	7	0	0	0	0
Low-temperature water radiator (window)	0	3	0	0	0
Low-temperature water radiator (backwall)	1	1	0	0	0

the occupancy zone, as well as the number of points in the zone,  $n$ , for which the PPD exceeded the permitted value of 10%. The number of points for which the PPD was calculated, for each simulation, was 60, thus giving a total of 720 values per heat source for the totality of the simulations.

Looking at the mean values of the PPD, we find that they are highly clustered, and always less than 10%. On the other hand, if we look at the maximum values of the PPD, or again those of  $n$ , some differences begin to appear. For example, the heated ceiling produced a much less comfortable thermal ambience than the other heat sources. Also, although it is true that, regarding consumption, the best results for the localized heat sources were obtained when they were positioned on the back wall, the same was not true for thermal comfort, due to the effect of cold radiation from the façade.

Overall thermal comfort is the index which gives us our first elements of comparison, but it is also interesting to look at the results obtained for local discomfort.

Table 8 gives the number of points for which the criteria of local discomfort were not respected. Let us recall that these criteria are:

- $R_h$ : horizontal radiant asymmetry (180 computed values per heat source);
- $R_v$ : vertical radiant asymmetry (180 computed values per heat source);
- $C$ : air currents (720 computed values per heat source);
- $E$ : air vertical temperature difference, feet-head (180 computed values per heat source);
- $S$ : floor temperature.

The  $E$  and  $S$  criteria were never violated. This result is in keeping with the experimental results found by Olesen *et al.* [6]. As to the  $R_h$ , it was of course greater in the case of the localized heat sources, whose radiative component was non-negligible. It would seem that the  $R_v$  was not a criterion that needed to be taken into account, except for the heated-floor system. Finally, we did not observe any problems due to air currents other than with the dis-

tributed heat sources, this being due to the cold boundary layer that developed along the façade.

## 7. CONCLUSIONS AND DISCUSSION

In this study, we have developed a simplified model for the thermal behavior of dwelling-cells. The basic principle of the model is that of a zonal representation of thermal exchanges within heated spaces.

After an experimental validation of the model, we carried out a numerical study which allowed us to compare the performances of different heating systems from the point of view of energy consumption and thermal comfort.

The results obtained indicate that the hot-water heated-floor system provides a good compromise between energy consumption and thermal comfort; which, if we were to draw up a list of rankings, would place this system slightly ahead of the others.

The electrical heated ceiling gave energy consumption figures equivalent to those of the hot-water heated floor, but its level of thermal comfort was slightly lower, due to the greater heterogeneity of the indoor thermal ambience.

Finally, for the localized heat sources, the level of thermal comfort was very satisfactory, but the energy consumption figures were slightly higher than those of the distributed heat sources, on account of the direct thermal coupling between the heat source and the heat-losing walls. Positioning localized heat sources on the back wall made it possible to reduce this difference but it will increase the downdraught.

Of course, the values of these parameters will vary according to the particular case under consideration, and we shall need to extend the investigation to other geometrical and thermal configurations in order to verify that the validity of our model does indeed continue to be confirmed by experience.

**Acknowledgements**—The authors would like to thank the members of the Groupe de Recherche sur les Emetteurs de Chaleur (GREC) for their cooperation.

## REFERENCES

1. *ASHRAE Handbook, Fundamentals*. ASHRAE, Atlanta, U.S.A., 1993.
2. *CIBSE, CIBSE Guide-Volume A*, Section A5. Chartered Institution of Building Services Engineers, London, U.K., 1986.
3. CSTB, Règles Th-C, Règles de calcul du coefficient de performance thermique globale des logements. *Cahiers du CSTB*, livraison no. 291, Cahier 2259, Paris, France, 1988.
4. Moderate thermal environments. Determination of the PMV and PPD indices and specification for thermal comfort. *ISO 7730*. International Standards Organization. Geneva, Switzerland, 1995.

5. Hannay, J., Laret, L., Lebrun, J., Marret, D. and Nussgens, P., Thermal comfort and energy consumption in winter conditions. A new experimental approach. *ASHRAE Transactions, Part 1*, 1978, **84**, 150–175.
6. Olesen, B. W., Mortensen, E., Thorshauge, J. and Berg-Munch, B., Thermal comfort in a room heated by different methods. *ASHRAE Transactions, Part 1*, 1980, **86**, 34–48.
7. Fanger, P. O., Ipsen, B. M., Langkilde, G., Olesen, B. W., Christensen, N. K. and Tanabe, S., Comfort limits for asymmetric thermal radiation. *Energy and Buildings*, 1985, **8**, 225–236.
8. Fanger, P. O., Banhidi, L., Olesen, B. W. and Langkilde, G., Comfort limits for heated ceiling. *ASHRAE Transactions, Part 2*, 1980, **86**, 141–156.
9. Morant, M. A. and Strengart, M., Simulation of hydronic heating system: radiator modelling. *Proceedings of CLIMA 2000*. Sarajevo, 1985, pp. 725–729.
10. Stephan, W., System simulation: radiator. *International Energy Agency, Annex 10*. University of Stuttgart, 1985.
11. Inard, C., Contribution à l'étude du couplage thermique entre une source de chaleur et un local. Thèse de doctorat, INSA de Lyon, France, 1988.
12. Barles, P., Caractérisation de l'émission thermique des convecteurs électriques. Etude statistique. *Rapport de contrat ADEME/CETIAT*. CETIAT, France, 1992.
13. Caccavelli, D., Francois, C., Maalej, J. et Zhao, H., Modélisation du comportement thermique d'un plafond chauffant. *Rapport de contrat ADEME/CSTB*. CSTB, France, 1993.
14. Liburdy, J. and Faeth, G. M., Heat transfer and mean structure of a turbulent thermal plume along a vertical isothermal wall. *Journal of Heat Transfer*, 1978, **100**(5), 177–183.
15. Lebrun, J. and Marret, D., Convection exchanges inside a dwelling room in winter. *Proceedings of the International Seminar of the International Center for Heat and Mass Transfer*. Dubrovnik, 1977, pp. 417–227.
16. Inard, C., Molle, N. et Allard, F., Etude du couplage thermique entre des corps de chauffe et un local: analyse expérimentale des échanges convectifs et de la structure moyenne du panache. *Revue Générale de Thermique*, 1991, **30**(351), 156–162.
17. Barles, P., Confort thermique et consommations énergétiques du chauffage par convecteur électrique. *Rapport de contrat EDF/CETIAT*. CETIAT, France, 1992.
18. Allard, F., Inard, C. et Simoneau, J. P., Phénomènes convectifs intérieurs dans les cellules d'habitation. Approches expérimentales et numériques. *Revue Générale de Thermique*, 1990, **29**(340), 216–225.
19. Olusoji, O. and Hetherington, H. J., Application of the finite element method to natural convection heat transfer from the open vertical channel. *International Journal of Heat and Mass Transfer*, 1977, **20**, 1195–1204.
20. Howarth, A. T., Temperature distributions and air movements in rooms with a convective heat source. Ph.D. thesis, University of Manchester, U.K., 1980.
21. Lebrun, J., Exigences physiologiques et modalités physiques de la climatisation par source statique concentrée. Thèse de doctorat, Université de Liège, Belgique, 1970.
22. *ASHRAE Handbook, HVAC Systems and Equipment*. ASHRAE, Atlanta, U.S.A., 1996.
23. Kast, W. and Klan, M., Auslegung und Prüfung von Fußbodenheizungen. *VDI Berichte*, 1982, **464**, 39–49.
24. Allard, F., Contribution à l'étude des transferts de chaleur dans les cavités thermiquement entraînées à grand nombre de Rayleigh. Thèse d'état, INSA de Lyon, France, 1987.
25. Sparrow, E. M. and Cess, R. D., *Radiation Heat Transfer*, Brooks/Cole Publishing Company, CA, 1970.
26. Maalej, J., Emetteurs de chaleur dans les bâtiments et étude des performances. Thèse de doctorat, Université de Valenciennes et du Haut Cambrésis, France, 1994.
27. Marret, D., Qualité de la ventilation mécanique contrôlée. Influence du mode de chauffage sur le confort et les pertes thermiques dans l'habitat. Thèse d'état, INSA de Lyon, France, 1981.